Tunable Nanochannels Fabricated by Mechanical Wrinkling/Folding of a Stiff Skin on a Soft Polymer

So Nagashima, Hamid Ebrahimi, Kwang-Ryeol Lee, Ashkan Vaziri, and Myoung-Woon Moon**

Nanochannels can effectively be used for manipulating nanomaterials, such as DNA,[1–6] proteins,[7,8] and nanoparticles.[9] Nanolithography-based methods, including electron-beam lithography,[10,11] focused ion beam (FIB) patterning,[12,13] and nanoimprint lithography,[14,15] have been widely used for the fabrication of nanochannels owing to their excellent patterning resolution, reproducibility, and flexibility. However, they often involve multistep processes with costly equipment and expertise, and therefore, are not readily accessible. Alternative methods that exploit thin film instabilities (e.g., surface wrinkling[8,16] and cracking[17–19] have been proposed to overcome the abovementioned limitations. Surface wrinkles appear when a thin stiff skin attached to a soft substrate (e.g., poly(dimethylsiloxane) (PDMS)) is compressed beyond a critical value,[20] while surface cracks emerge in the same physical system as a result of strain energy release due to mechanical fracture of the stiff skin.[19] The formed patterned surfaces can be used to create closed channels when they are used with a sealing material such as PDMS or glass. However, the sealing process generally requires relatively high external forces to ensure proper bonding, resulting in distortion of the original wrinkled or cracked surface morphology. Moreover, the sealing material cannot easily be removed because of its strong adhesion to the counter surface. The process is thus irreversible and direct analysis of the fluids or materials inside the channels is infeasible.

Here, we present a straightforward method for fabricating nanochannels that exploits another type of thin film instability called folding, which emerges during post-instability evolution of surface wrinkles.[21–24] In our experiments, a flat PDMS substrate was uniaxially stretched and treated with oxygen plasma for varying durations, resulting in formation of a stiff-oxidized skin of varying thickness on the surface.[25] Thereafter, the stretch was released to induce a compressive strain (ε), defined as the change in length per unit of the initial length of the substrate, in the skin. At small strain levels, wrinkles appeared on the substrate surface, forming open channels with a specific wavelength and amplitude (**Figure 1**a). Further increase in the strain level triggered the transition from wrinkles to folds, creating well-defined closed channels with a diameter in the nanoscale range (Figure 1b). The characteristic dimensions of the channels such as wavelength, amplitude, and diameter were robustly tunable by changing the duration of oxygen plasma treatment and strain level. Furthermore, the configuration of the channels was switchable from open to closed and vice versa by controlling the strain level. We demonstrated a unique application of the tunable nanochannels for "on demand" trapping and releasing gold (Au) nanoparticles.

Surface morphological changes of a substrate treated with oxygen plasma for 20 min were analyzed by in situ atomic force microscopy (AFM) with respect to the nominal strain induced in the skin. The surface morphology can be categorized into three distinctive regimes: wrinkling, transition, and folding (**Figure 2**a). In the first regime, wrinkles were observed on the surface, and the wavelength (λ_W) was decreased in a relatively linear fashion with an increase in the nominal strain (Figure 2b), while the amplitude (A_W) was increased approximately with the square root of the nominal strain (Figure 2c). When a PDMS substrate is subjected to large deformation, the wavelength decreases while the amplitude increases with increasing strain

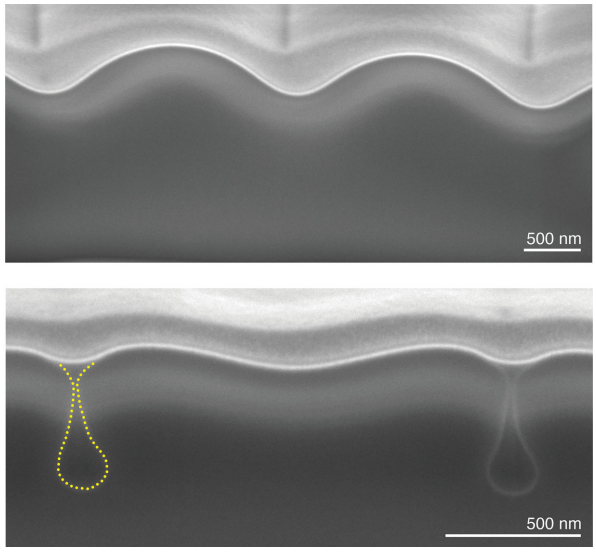

Figure 1. Morphological instabilities of a stiff skin formed on soft PDMS substrates. Cross-sectional scanning electron microscope (SEM) images of a) open channels formed by wrinkling instability (ε = –0.12) and b) closed ones created by folding instability (ε = –0.53). These samples were prepared by 10 min oxygen plasma treatment at a power of 200 W. The images were obtained at a tilt angle of 52°.

Dr. S. Nagashima, Dr. K.-R. Lee, Dr. M.-W. Moon
Institute for Multidisciplinary Convergence of Matter
Korea Institute of Science and Technology
Seoul 136–791, Republic of Korea
E-mail: mwmoon@kist.re.kr
H. Ebrahimi, Prof. A. Vaziri
Department of Mechanical and Industrial Engineering
Northeastern University
Boston, Massachusetts 02115, USA
E-mail: vaziri@coe.neu.edu

DOI: 10.1002/admi.201400493

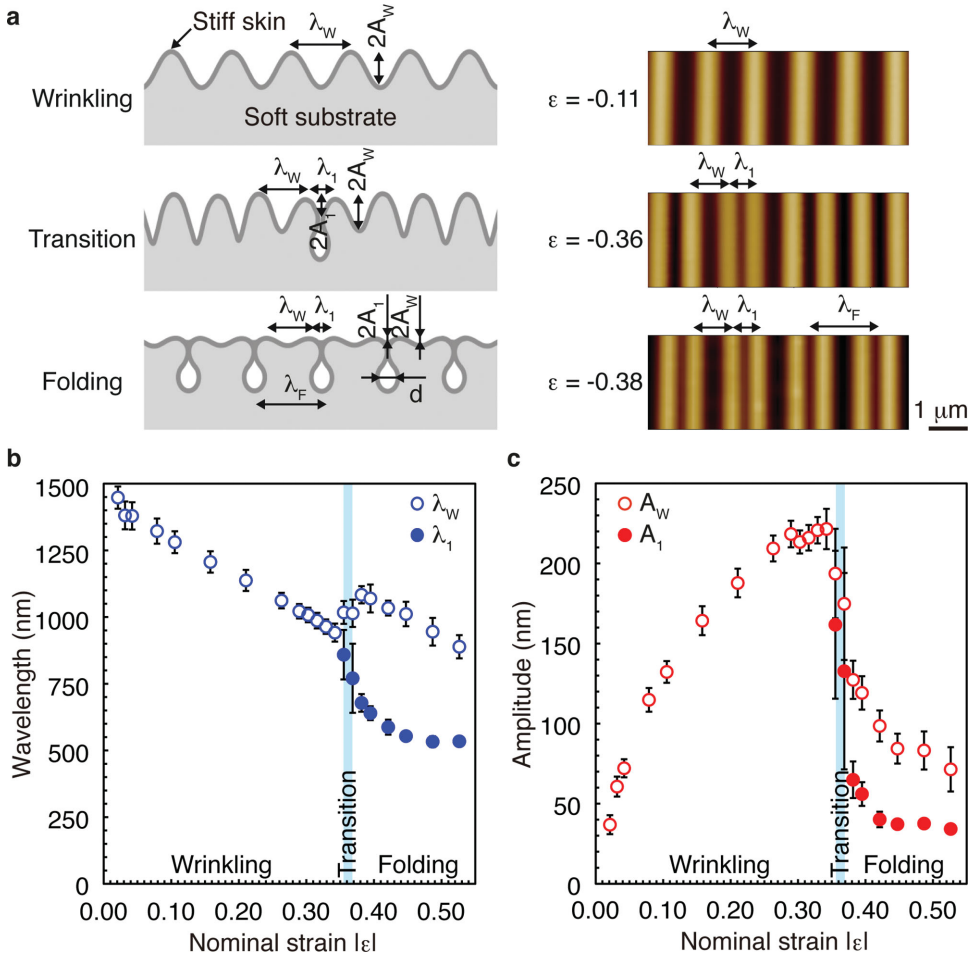

Figure 2. Evolution of surface morphology as a function of the nominal strain applied. a) Schematic illustrations of the representative surface morphologies and the corresponding AFM images acquired at various nominal strains: $\varepsilon = -0.11$ (top: wrinkling); $\varepsilon = -0.36$ (middle: transition); $\varepsilon = -0.38$ (bottom: folding). b,c) The wavelength(s) (λ_W, λ_1) and amplitude(s) (A_W, A_1) were measured for a PDMS substrate treated with oxygen plasma for 20 min. The blue shadowing indicates the regime of transition from wrinkling to folding.

level.[26] In this study, the transition from wrinkles to folds started at the nominal strain of approximately –0.36. During the transition regime, some of the wrinkles moved toward their neighboring wrinkles, creating a new morphology consisting of wrinkles and folds characterized by wavelengths (λ_W, λ_1) and amplitudes (A_W, A_1). The surface morphology during the transition regime depends on the relative Young's moduli of the skin (E_{skin}) and the substrate (E_{sub}), and such a coexistence of wrinkles with folds has been reported for a bilayer polymeric system under biaxial compressive stress, where $10^2 < E_{skin}/E_{sub} \leq 10^3$.[23] Here, Young's moduli of the PDMS substrate and the stiff skin used in this study are ≈0.5 MPa[27] and ≈1.5 GPa,[28] respectively, yielding $E_{skin}/E_{sub} \approx 10^3$.

When the nominal strain was further increased, the complete transition to folds eventually occurred with characteristic wavelengths (λ_F, λ_W, λ_1) and amplitudes (A_W, A_1), where $\lambda_F = \lambda_W + \lambda_1$. In the folding regime, two adjacent wrinkles evolved to create a single fold, where the wavelength of folds right after the transition was approximately equal to twice that of wrinkles prior to the transition, i.e., $\lambda_F \approx 2\lambda_W$. As can be seen, the value of λ_1 saturated with an increase in the nominal strain, whereas λ_W was decreased from 1084 to 889 nm. Similarly, A_1 was decreased from 65 to 34 nm, not displaying a strong dependence on the nominal strain, while A_W was significantly decreased from 127 to 71 nm with an increase in the strain. Although a higher order bifurcation, i.e., a period-quadrupling mode, has been reported,[22,24] it was not observed in this study even at a high level of compressive strain. This behavior would probably be due to the high level of stretch applied to the substrate prior to formation of the stiff skin. The surface morphological evolution of a system consisting of a stiff layer and a soft substrate is significantly affected by pre-stretch of the substrate and its level (Table S1, Supporting Information). In addition, the critical strains for post-wrinkling bifurcations are shifted to higher levels with increasing pre-stretch ratio.[29,30] In this study, the stiff skin was formed on the surface of pre-stretched PDMS substrates by oxygen plasma treatment, and various levels of compressive strain were induced by release of the pre-stretch. The prestretch ratio employed here was 111%, which is the highest among the values reported.[24,29,30] The onset of period-quadrupling mode would thus be delayed to a strain level higher than the others reported to date, which

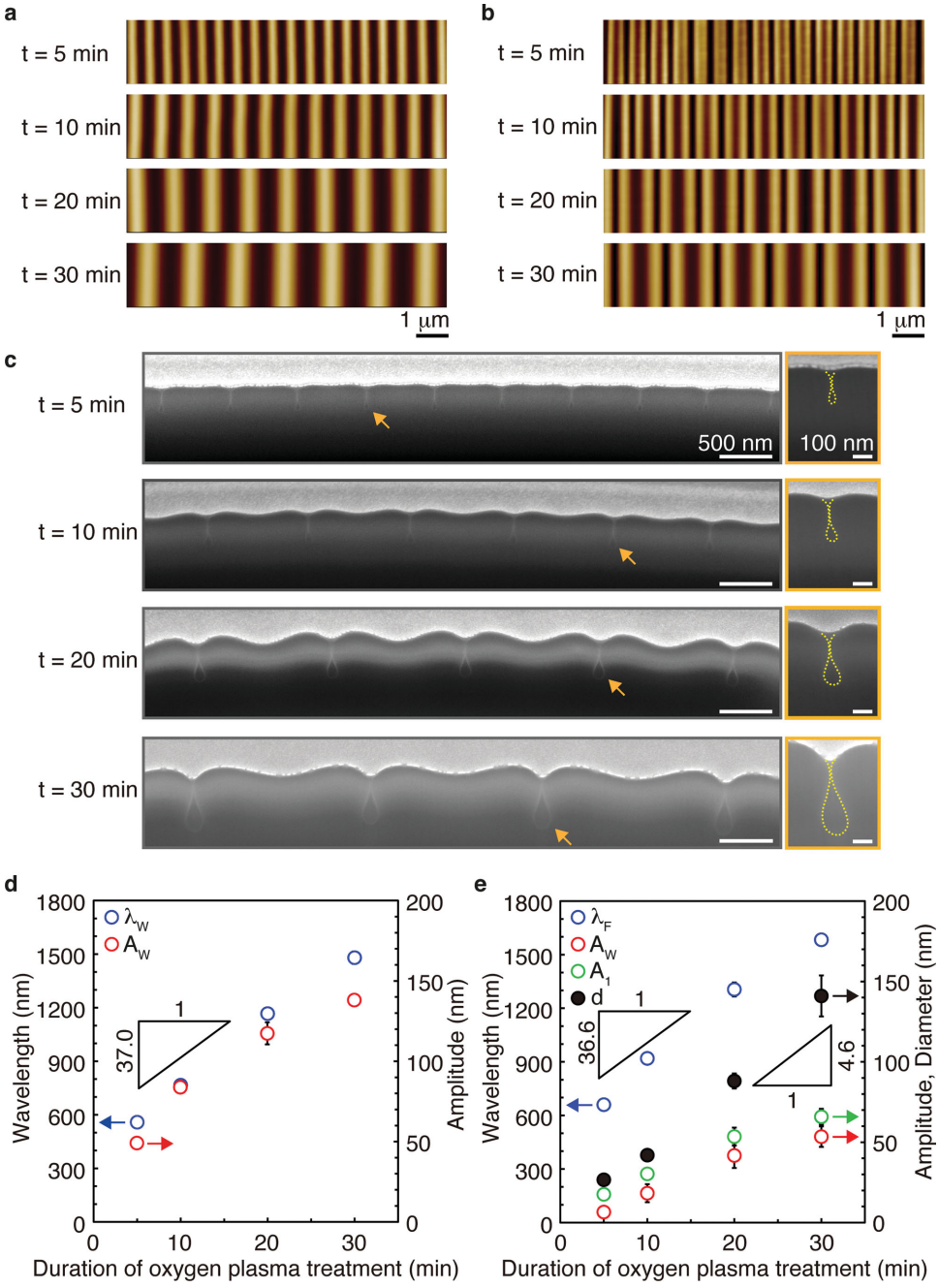

Figure 3. Evolution of surface morphology as a function of the duration of oxygen plasma treatment. Representative AFM images of PDMS substrates treated with oxygen plasma for varying durations, followed by compression at the strains of a) $\varepsilon = -0.08$ and b) $\varepsilon = -0.53$. c) Cross-sectional SEM images of PDMS substrates treated with oxygen plasma for 5 to 30 min, followed by compression at the nominal strain of $\varepsilon = -0.53$. A magnified image of a closed channel of each sample indicated by the orange arrow is shown next to the original image. These images were obtained at a tilt angle of 52°. d) The wavelength (λ_W) and amplitude (A_W) of the wrinkles formed at the strain of $\varepsilon = -0.08$ as a function of the duration of oxygen plasma treatment. e) The wavelength (λ_W, λ_F), amplitudes (A_1, A_W), and diameter (d) of the folds created at the strain of $\varepsilon = -0.53$ as a function of the duration of oxygen plasma treatment.

could be over the range of compressive strain investigated here. Note that the folding behavior of the stiff skin can be affected by the release rate of the pre-stretch applied to the PDMS substrates (Figure S1, Supporting Information), and release rates appropriate for the formation of well-defined folds were employed here.

Figure 3a,b shows the AFM images of surfaces compressed at nominal strains of –0.08 and –0.53 after oxygen plasma treatment for varying durations, respectively, and Figure 3c presents the cross-sectional SEM images of the samples compressed at the nominal strain of –0.53. With increasing duration of oxygen plasma treatment from 5 to 30 min, the

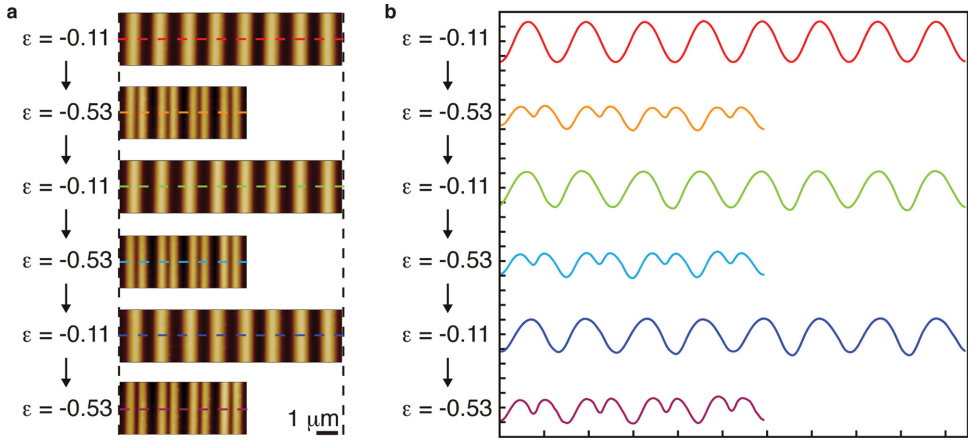

Figure 4. Surface morphological changes with repeated compression/stretch. a) AFM images of a PDMS substrate surface treated with oxygen plasma for 20 min obtained at various strain levels. b) The surface profile analyzed by in situ AFM at various strain levels. Each tick mark on the horizontal and vertical axes denotes 1 μm and 100 nm, respectively.

wavelength (λ_W) and amplitude (A_W) of wrinkles increased from 559 to 1480 nm and from 49 to 138, respectively, as quantified in Figure 3d. In particular, the increase in the wavelength was in a relatively linear fashion with a slope of 37.0. The wavelength and amplitude of wrinkles are expressed as a function of the thickness of a stiff skin.[31,32] Here, λ_W increased linearly with increasing duration of oxygen plasma treatment up to 20 min, implying a linear increase in the skin thickness. However, λ_W showed the initiation of a saturated behavior with a further increase in the duration of oxygen plasma treatment. This saturation can be accounted for by the limited increase in the skin thickness during oxygen plasma treatment.[33] Similarly, the wavelength of folds (λ_F) increased approximately linearly from 660 to 1584 nm as the duration of oxygen plasma treatment was increased, where the proportionality constant measured 36.6 (Figure 3e). The primary (A_1) and secondary (A_W) amplitudes of the folds also increased from 18 to 66 nm and from 7 to 53 nm, respectively. These results suggest that λ_F, A_1, and A_2 are also a function of the skin thickness, indicating that one can control the dimensions of folds simply by changing the duration of oxygen plasma treatment.

Figure 3c reveals arrays of closed channels with a teardrop shape created by the contact of adjacent wrinkles. The diameter of closed channels (d) was measured using ImageJ (National Institutes of Health, USA) and plotted with respect to the duration of oxygen plasma treatment (Figure 3e), showing that the channel diameter increased with increasing duration. This relationship can be explained by a simple geometrical argument based on conservation of the total length of the skin. Assuming that the cross sections of the closed channels are perfectly round in shape and the top surface is flat, i.e., $d \gg A_1, A_W$, the following equation can be derived:

$$\pi d = L_0 - \lambda_F \tag{1}$$

where L_0 is the unit length of the skin before compression. Since $\varepsilon = (\lambda_F - L_0)/L_0$, Equation (1) can be rearranged as:

$$d = -\frac{\varepsilon}{(1+\varepsilon)\pi}\lambda_F \tag{2}$$

Here, the actual cross sections of the closed channels are teardrop shaped and the wavelength of folds is a function of the duration of oxygen plasma treatment, as revealed in Figure 3e. Therefore, Equation (2) can yield the equation below:

$$d \approx \beta \frac{\varepsilon}{(1+\varepsilon)\pi} t \tag{3}$$

where β and t denote a prefactor and the duration of oxygen plasma treatment, respectively. Equation (3) shows good agreement with our experimental results with $\beta \approx -12.9$.

The surface morphological changes with repeated increase and decrease in the strain were analyzed by in situ AFM. **Figure 4**a,b shows the representative AFM images of a surface area obtained at different strain levels and the corresponding surface profiles, respectively. With an increase in the strain from –0.11 to –0.53, the surface morphology evolved from wrinkles to folds, which is in agreement with the results shown in Figure 2. When the strain was reduced from –0.53 to –0.11, the folds changed to wrinkles. The morphological transition between wrinkles and folds was repeatedly achieved as shown in Figure 4. These results clearly demonstrate that the open/closed configuration of the channels is reversibly switchable by controlling the strain level.

By taking advantage of the tunable nanochannels, one can easily place nanomaterials in the closed channels by either trapping or growing them inside. In this study, we used Au nanoparticles, which have found various applications in biomedical fields, such as diagnosis, therapy, and imaging,[34,35] to demonstrate the potential usage of tunable nanochannels. **Figure 5**a presents a series of AFM images of the nanoparticles dispersed on the surface obtained at various strain levels, and Figure 5b shows the corresponding surface profiles for nanoparticles in wrinkled (A) and folded (B) regions. At the strain of –0.24, the nanoparticles A and B were preferentially aligned along the troughs of the wrinkles. When the strain was increased from

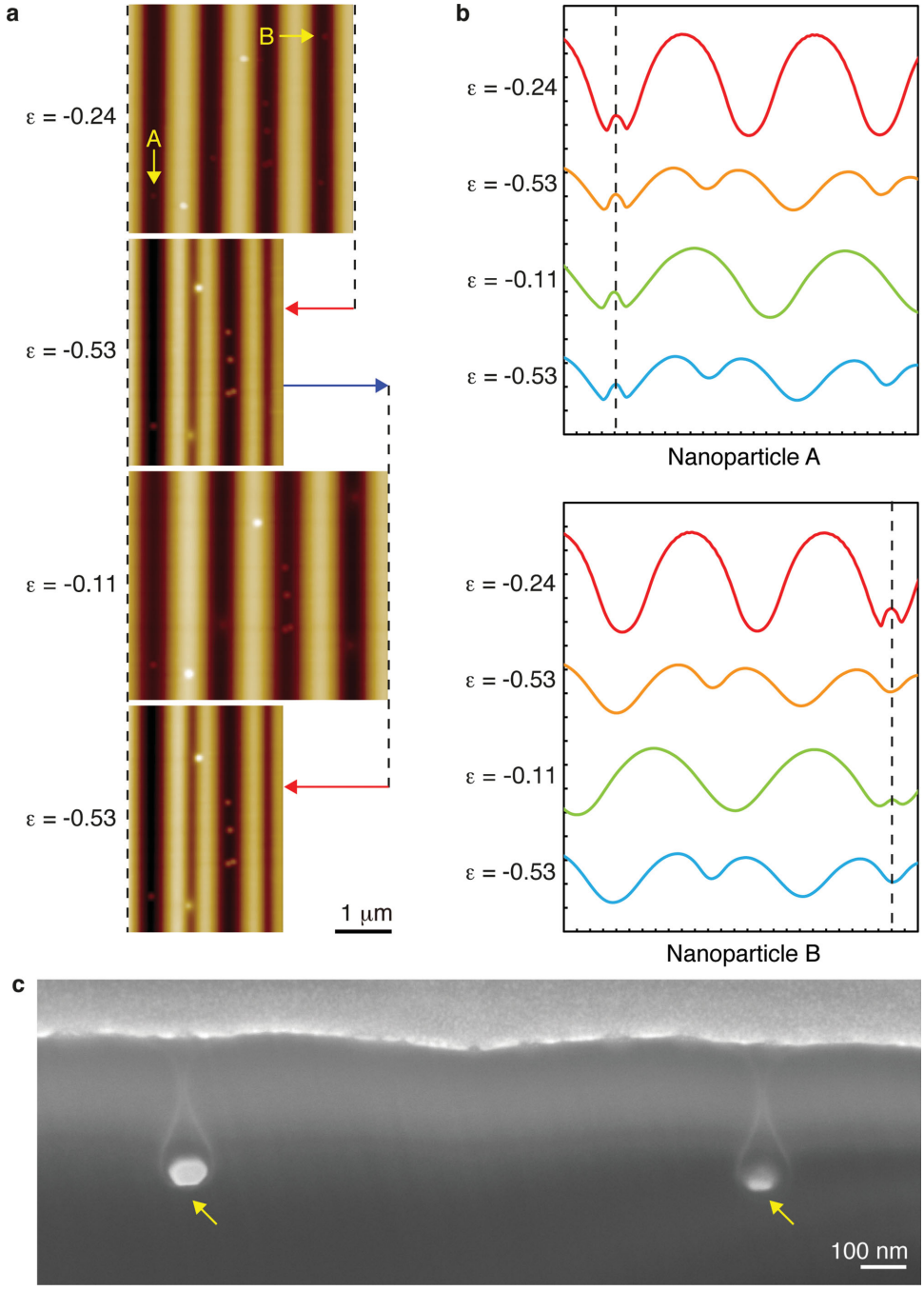

Figure 5. Trapping and release of Au nanoparticles using the tunable nanochannels. a) AFM images of Au nanoparticles on the surface of a PDMS substrate treated with oxygen plasma for 20 min obtained at various strain levels. The red and blue arrows indicate compression and stretch, respectively. b) The surface profile analyzed by in situ AFM at various strain levels. The nanoparticle A was in a wrinkled region, while the nanoparticle B was in a folded one. The dashed lines indicate the location of the nanoparticles A and B. Each tick mark on the horizontal and vertical axes denotes 100 nm. c) A cross-sectional SEM image of Au nanoparticles trapped in the closed channels, indicated by the yellow arrows, formed at the strain of $\varepsilon = -0.53$. This image was obtained at a tilt angle of 52°.

–0.24 to –0.53, the nanoparticle A remained detectable on the surface, whereas the nanoparticle B was concealed in a closed channel (Figure 5c). As the strain was decreased to –0.11, the nanoparticle B appeared on the surface again because of the surface morphological transition from folds to wrinkles. With increasing strain to –0.53, the nanoparticle B was hidden beneath the surface again. This process is repeatable by the simple control of the strain level, providing a robust method for trapping and revealing nanoparticles "on demand". The diameter of the nanoparticles used here was comparable to that of the nanochannels employed for this experiment, and each channel accommodated a single nanoparticle. Note that the

technique discussed above can also be used to trap nanoparticles with a higher concentration and/or a smaller diameter (Figure S2, Supporting Information).

In summary, we have shown that nanochannels can easily be fabricated by the facile method based on mechanical wrinkling/folding of the stiff skin formed on the surface of soft PDMS substrates by oxygen plasma treatment. The characteristic dimensions of the nanochannels such as wavelength, amplitude, and diameter are robustly tunable by changing the duration of oxygen plasma treatment and the level of strain applied to the skin. Furthermore, the open/closed configuration of the nanochannels is reversibly switchable by controlling the applied strain, and we have demonstrated "on demand" trapping and release of Au nanoparticles using the tunable nanochannels. The characteristic length of the arrays of nanochannels is limited to the tens of micrometer scale (Figure S3, Supporting Information) because of the presence of structural defects and cracks. However, owing to the facile tunability, the nanochannels containing Au nanoparticles could effectively be used to construct a 3D platform for specific biomedical applications. Moreover, the switchable configuration of the nanochannels allows for subsequent direct analysis of the materials of interest trapped inside the closed channels.

Experimental Section

Formation of Surface Wrinkles and Folds: PDMS prepolymer was prepared by a mixture of silicone elastomer base with a curing agent at a ratio of 20:1 by weight (Sylgard 184, Dow Corning Corp.). Prior to curing, the air bubbles trapped were removed in a vacuum chamber. The mixture was cured at 70 °C for 2 h, and the resulting PDMS sheet with a thickness of 1.5 mm was cut into substrates of 10×25 mm^2. Each PDMS substrate was stretched uniaxially up to ≈111% of the initial length and subsequently treated with oxygen plasma for 5 to 30 min with a low-pressure plasma system (COVANCE, Femto Science) to form a stiff-oxidized skin of varying thickness on the surface.[25] The flow rate, power, and working pressure during the plasma treatment were 20 sccm, 100 or 200 W, and ≈0.6 Torr, respectively. Afterwards, the stretch applied to the substrate was released to induce a nominal compressive strain, defined as the change in length per unit of the initial length of the substrate, in the skin. The nominal strain varied according to the level of the release of stretch, and complete release of the stretch corresponded to the nominal strain of –0.53. Surface morphology of the samples was analyzed by in situ AFM (XE-70, Park Systems Corp.) in noncontact mode. Cross sections of the samples were observed with a high-resolution SEM equipped with focused ion beam (FIB; NOVA200, FEI). Prior to imaging, the samples were coated with platinum to prevent any possible alteration of the surface morphology and any potential damage by gallium ion irradiation.

Dispersion of Au Nanoparticles: The surface of a stretched PDMS substrate was treated with oxygen plasma for 20 min and subsequently modified with 10 µL of poly-D-lysine in borate buffer for 2 min, followed by gentle rinse with distilled water and dry with N_2 gas. The initial stretch was then partially released to create wrinkles on the surface, where the nominal strain measured about –0.24. For dispersion of the nanoparticles, spin coating, which can effectively be used for assembling colloidal particles on wrinkled surfaces,[36–39] was employed. A droplet (2.5 µL) of a solution containing Au nanoparticles with a mean diameter of 100 nm (Sigma-Aldrich) was dispersed on the wrinkled surface by a two-step spin coating; the first step was performed at 200 rpm for 60 s, followed by the second step at 2000 rpm for 30 s. Afterwards, the nominal strain was varied and the distribution of the nanoparticles on the surface was characterized with respect to the strain by in situ AFM. To analyze the distribution of the nanoparticles inside the folds, or closed channels, cross sectioning using FIB was performed.

Supporting Information

Supporting Information is available from the Wiley Online Library or from the author.

Acknowledgements

This work was supported by the KIST internal project (2E31230), the Global Excellent Technology Innovation R&D Program of the Ministry of Knowledge Economy (MKE), the Republic of Korea, and Project No. 10040003 funded by the MKE. A.V. and H.E. are thankful for the support of NSF (CMMI-1149750). The authors thank Dr. Ji Yeong Lee and Mr. Ki-Hoon Park at KIST for their expert assistance for cross-sectional imaging.

Received: October 31, 2014
Published online: November 25, 2014

[1] J. O. Tegenfeldt, H. Cao, W. W. Reisner, C. Prinz, R. H. Austin, S. Y. Chou, E. C. Cox, J. C. Sturm, *Biophys. J.* **2004**, *86*, 596A.
[2] J. O. Tegenfeldt, C. Prinz, H. Cao, R. L. Huang, R. H. Austin, S. Y. Chou, E. C. Cox, J. C. Sturm, *Anal. Bioanal. Chem.* **2004**, *378*, 1678.
[3] R. Riehn, M. C. Lu, Y. M. Wang, S. F. Lim, E. C. Cox, R. H. Austin, *Proc. Natl. Acad. Sci. USA* **2005**, *102*, 10012.
[4] J. T. Mannion, C. H. Reccius, J. D. Cross, H. G. Craighead, *Biophys. J.* **2006**, *90*, 4538.
[5] Y. H. Cho, S. W. Lee, T. Fuji, B. J. Kim, *Microelectron. Eng.* **2008**, *85*, 1275.
[6] E. Angeli, C. Manneschi, L. Repetto, G. Firpo, U. Valbusa, *Lab Chip* **2011**, *11*, 2625.
[7] P. Sivanesan, K. Okamoto, D. English, C. S. Lee, D. L. DeVoe, *Anal. Chem.* **2005**, *77*, 2252.
[8] S. Chung, J. H. Lee, M.-W. Moon, J. Han, R. D. Kamm, *Adv. Mater.* **2008**, *20*, 3011.
[9] K. Efimenko, M. Rackaitis, E. Manias, A. Vaziri, L. Mahadevan, J. Genzer, *Nat. Mater.* **2005**, *4*, 293.
[10] S. H. Kim, Y. Cui, M. J. Lee, S. W. Nam, D. Oh, S. H. Kang, Y. S. Kim, S. Park, *Lab Chip* **2011**, *11*, 348.
[11] S. W. Nam, M. H. Lee, S. H. Lee, D. J. Lee, S. M. Rossnagel, K. B. Kim, *Nano Lett.* **2010**, *10*, 3324.
[12] M. W. Moon, S. H. Lee, J. Y. Sun, K. H. Oh, A. Vaziri, J. W. Hutchinson, *Proc. Natl. Acad. Sci. USA* **2007**, *104*, 1130.
[13] M. W. Moon, J. H. Han, A. Vaziri, E. K. Her, K. H. Oh, K. R. Lee, J. W. Hutchinson, *Nanotechnology* **2009**, *20*, 115301.
[14] L. J. Guo, X. Cheng, C. F. Chou, *Nano Lett.* **2004**, *4*, 69.
[15] Y. H. Cho, J. Park, H. Park, X. Cheng, B. J. Kim, A. Han, *Microfluid. Nanofluid.* **2010**, *9*, 163.
[16] H. S. Kim, A. J. Crosby, *Adv. Mater.* **2011**, *23*, 4188.
[17] X. Y. Zhu, K. L. Mills, P. R. Peters, J. H. Bahng, E. H. Liu, J. Shim, K. Naruse, M. E. Csete, M. D. Thouless, S. Takayama, *Nat. Mater.* **2005**, *4*, 403.
[18] K. L. Mills, D. Huh, S. Takayama, M. D. Thouless, *Lab Chip* **2010**, *10*, 1627.
[19] H. N. Kim, S. H. Lee, K. Y. Suh, *Lab Chip* **2011**, *11*, 717.
[20] D.-Y. Khang, J. A. Rogers, H. H. Lee, *Adv. Funct. Mater.* **2009**, *19*, 1526.
[21] L. Pocivavsek, R. Dellsy, A. Kern, S. Johnson, B. H. Lin, K. Y. C. Lee, E. Cerda, *Science* **2008**, *320*, 912.

[22] F. Brau, H. Vandeparre, A. Sabbah, C. Poulard, A. Boudaoud, P. Damman, *Nat. Phys.* **2011**, *7*, 56.
[23] P. Kim, M. Abkarian, H. A. Stone, *Nat. Mater.* **2011**, *10*, 952.
[24] J. Y. Sun, S. M. Xia, M. W. Moon, K. H. Oh, K. S. Kim, *Proc. R. Soc. A* **2012**, *468*, 932.
[25] M. W. Moon, A. Vaziri, *Scr. Mater.* **2009**, *60*, 44.
[26] H. Q. Jiang, D. Y. Khang, J. Z. Song, Y. G. Sun, Y. G. Huang, J. A. Rogers, *Proc. Natl. Acad. Sci. USA* **2007**, *104*, 15607.
[27] J. Yin, X. Han, Y. P. Cao, C. H. Lu, *Sci. Rep.* **2014**, *4*, 5710.
[28] S. Béfahy, P. Lipnik, T. Pardoen, C. Nascimento, B. Patris, P. Bertrand, S. Yunus, *Langmuir* **2010**, *26*, 3372.
[29] Y. P. Cao, J. W. Hutchinson, *J. Appl. Mech.* **2012**, *79*, 031019.
[30] A. Auguste, L. Jin, Z. Suo, R. C. Hayward, *Soft Matter* **2014**, *10*, 6520.
[31] N. Bowden, S. Brittain, A. G. Evans, J. W. Hutchinson, G. M. Whitesides, *Nature* **1998**, *393*, 146.
[32] R. Huang, *J. Mech. Phys. Solids* **2005**, *53*, 63.
[33] V. Z. H. Chan, E. L. Thomas, J. Frommer, D. Sampson, R. Campbell, D. Miller, C. Hawker, V. Lee, R. D. Miller, *Chem. Mater.* **1998**, *10*, 3895.
[34] E. Boisselier, D. Astruc, *Chem. Soc. Rev.* **2009**, *38*, 1759.
[35] L. Dykman, N. Khlebtsov, *Chem. Soc. Rev.* **2012**, *41*, 2256.
[36] S. Hiltl, M. P. Schurings, A. Balaceanu, V. Mayorga, C. Liedel, A. Pich, A. Boker, *Soft Matter* **2011**, *7*, 8231.
[37] S. Hiltl, J. Oltmanns, A. Boker, *Nanoscale* **2012**, *4*, 7338.
[38] M. Müller, M. Karg, A. Fortini, T. Hellweg, A. Fery, *Nanoscale* **2012**, *4*, 2491.
[39] C. Hanske, M. B. Muller, V. Bieber, M. Tebbe, S. Jessl, A. Wittemann, A. Fery, *Langmuir* **2012**, *28*, 16745.

